Scanning Electron Microscopy

Volume 1986 | Number 2 Article 12

7-15-1986

Capacitive Coupling Voltage Contrast

S. Görlich
Siemens Research Laboratories

K. D. Herrmann
Universität Duisburg

W. Reiners
Universität Duisburg

E. Kubalek
Universität Duisburg

Follow this and additional works at: https://digitalcommons.usu.edu/electron

Part of the Biology Commons

Recommended Citation

Görlich, S.; Herrmann, K. D.; Reiners, W.; and Kubalek, E. (1986) "Capacitive Coupling Voltage Contrast," *Scanning Electron Microscopy*: Vol. 1986 : No. 2 , Article 12.
Available at: https://digitalcommons.usu.edu/electron/vol1986/iss2/12

This Article is brought to you for free and open access by the Western Dairy Center at DigitalCommons@USU. It has been accepted for inclusion in Scanning Electron Microscopy by an authorized administrator of DigitalCommons@USU. For more information, please contact digitalcommons@usu.edu.

SCANNING ELECTRON MICROSCOPY/1986/II (Pages 447-464)
SEM Inc., AMF O'Hare (Chicago), IL 60666-0507 USA

0586-5581/86$1.00+05

CAPACITIVE COUPLING VOLTAGE CONTRAST

S. Görlich*, K.D. Herrmann, W. Reiners, E. Kubalek

Universität Duisburg, Fachgebiet Werkstoffe der Elektrotechnik
Leiter: Prof. Dr.-Ing. Erich Kubalek
Kommandantenstr. 60
4100 Duisburg 1, F.R.G.

* Now at Siemens Research Laboratories Munich, F.R.G.

(Received for publication March 07, 1986: revised paper received July 15, 1986)

Abstract

Capacitive coupling voltage contrast (CCVC) allows electron-beam testing of passivated integrated circuits (IC) without radiation damage or prior, time-consuming specimen preparation. This effect occurs when low primary electron energies are used and the electron yield of the passivation layer is greater than 1. Signal changes in the relevant interconnections are transferred to the passivation surface via capacitive coupling, but they vanish there within the storage time due to electron irradiation. A physical model explains the dependence of CCVC on three parameters: electron irradiation, the passivation material and the signals within the IC. Computer simulations based on this model describe the experimentally-obtained dependencies of the storage time with precision and allow predictions to be made for using CCVC in electron beam testing. The requisite modifications to the electron beam testing system are described and the possible uses of CCVC for testing passivated devices within IC are demonstrated on the basis of examples.

KEY WORDS: Capacitive coupling voltage contrast, electron beam testing, passivated integrated circuits, IC-internal voltage measurement, fast digital image acquisition system, multisampling system.

Address for correspondence:

E. Kubalek, Universität Duisburg, Fachgebiet Werkstoffe der Elektrotechnik,Kommandantenstr.60, 4100 Duisburg 1,F.R.G. Phone No.(0203) 379-3406

Introduction

Electron beam testing has proved to be a suitable testing tool in the development of new very large scale integrated (VLSI) devices/5,20/. Due to its internal chip access, this testing method is used in the design/redesign phase for design verification, fault localization, technological optimization and for checking computer simulations /4,20/. In these design applications, electron beam testing is applied to unpassivated IC, i.e., prior to the passivation process designed to protect the device.

Other fields in which electron beam testing is used are those of production and applications. The aim is to determine the causes of yield reductions, field failures and failures following load tests. But in these application areas the completed product - the passivated device - is tested.

In principle, the electron beam testing techniques developed for unpassivated devices may also be used when the passivation layer has been completely removed by plasma or chemical etching or when local measuring windows have been opened in the passivation layer /4/. These procedures have the disadvantage of possible device damage during preparation plus the fact that implementation of the process steps is time- and cost-intensive.

It is simpler to apply electron beam testing directly to a passivated device. Two effects lend themselves to this purpose: the conductivity induced by the electron beam in the insulator when using high primary electron energies /28/ and the capacitive coupling voltage contrast (CCVC) obtained when using low primary electron energies /3/.

The first effect has been known for many years and has been used in electron beam testing. Since the range of the primary electrons can be changed by suitably selecting their energy, signals on passivated interconnections can be measured by generating a "conductive channel" from the passivation layer to the interconnection. This method allows direct electron beam testing on passivated bipolar devices, since these are largely insensitive to the high-energy electron beam which must be used /6/. In contrast, serious radiation damage occurs when this beam is applied

directly to passivated MOS-devices /12,20/. Although methods have been developed which reduce this radiation damage (by blanking the electron beam during digital scanning in the region of the gate oxide in window scan mode /10/ or by automatically positioning the electron beam in vector scan mode /13/, the elaborate equipment and the high degree of automation required prevent their practical application.

The CCVC effect arising with low primary electron energies allows direct and nondestructive electron beam testing of passivated devices. It was described in 1974 by Crosthwait and Ivy /3/. With sufficiently low primary electron energies, the isolating passivation layer no longer becomes negatively charged and a voltage contrast is set up by way of capacitative coupling between the irradiated passivation surface and the interconnection below it /3,9/. The CCVC vanishes during a period known as the storage time after application of a voltage difference when the electron irradiation is continued /11,30/.

CCVC has been thoroughly investigated in the intervening period and a physical model has been presented to explain it /11/. A number of applications of this effect have also been described /9,16,29,30,31,33/. Both the fundamentals of CCVC and its potential applications are presented in this paper.

Fundamentals of CCVC

In the following, the CCVC effect is explained on the basis of a simple experiment and a physical model for it presented. This provides the starting point for a quantitative description of the effect obtained by computer simulations and specifying the exact temporal course of the CCVC as a function of a large number of relevant parameters. The storage time in particular, i.e. the time within which the effect can be observed, is calculated and compared with the experimental results. A number of theoretical predictions are made for applying CCVC to electron beam testing.

Fundamental experiments and qualitative models

Observations on various passivated IC and test structures show that in principle CCVC occurs in all the passivation layers investigated, such as silicon dioxide SiO_2, silicon nitride Si_3N_4 and polyimide PIQ, for all primary beam currents used in the region between 10^{-12} and 10^{-7} A when primary electron (PE) energies smaller than a specific energy E_{PEII} are selected. This upper energy level depends on the passivation material, the manufacturing process, the pretreatment of the surface by cleaning and on the radiation to which it has already been exposed. The value of E_{PEII} therefore varies according to the specimen, but is typically below 1.5 keV for all passivation layers. Larger PE energies give rise to strong, uncontrollable negative charging of the passivation surface which prevent the effect arising. Its occurrence therefore depends on the selection of suitably low PE energies.

A study of turnon and turnoff processes is particularly useful for obtaining an understanding of CCVC on the basis of a model. They are shown in the successive micrographs of a test structure in Fig. 1. This structure consists of three horizontal rows of linked aluminium pads. Only the right-side pads are passivated with 0.36 µm SiO_2, whereas the others are unpassivated. A PE energy of 1.3 keV was selected, only a little below the limiting energy E_{PEII}.

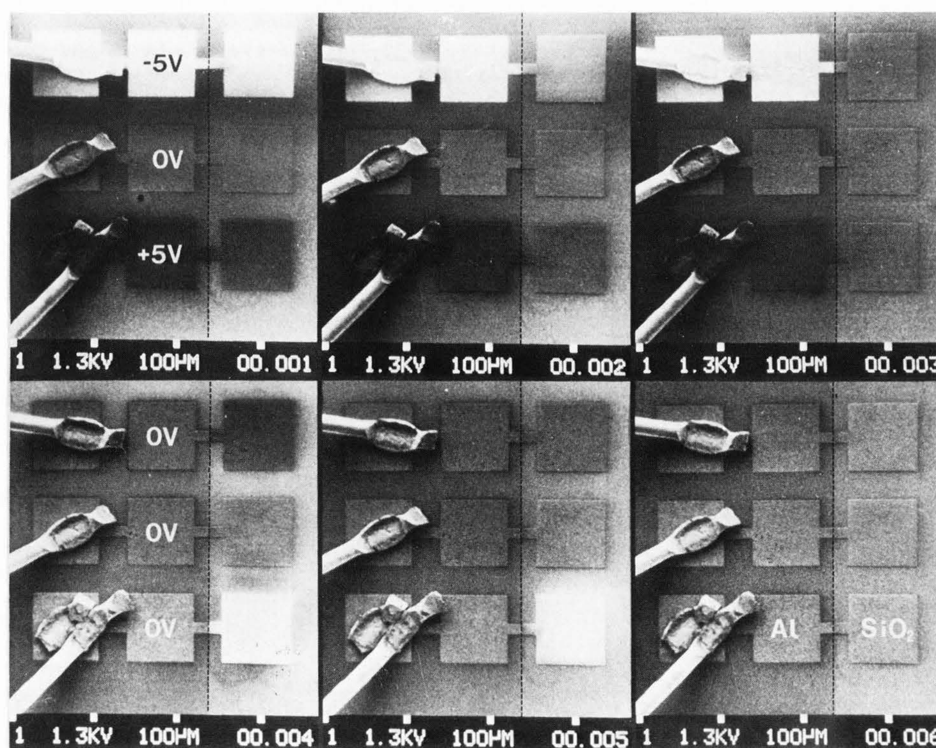

Fig. 1.1-1.6: Voltage contrast micrographs of nonpassivated pads (left: Al) and of pads passivated with 0.36 µm SiO_2 (right: SiO_2); successive recordings after turn on (1.1-1.3) and turn off (1.4-1.6) of +5 V and - 5 V; e-beam parameters : E_{PE} = 1.3 keV, I_{PE} = 10^{-9}A, exposure time was 1 s.

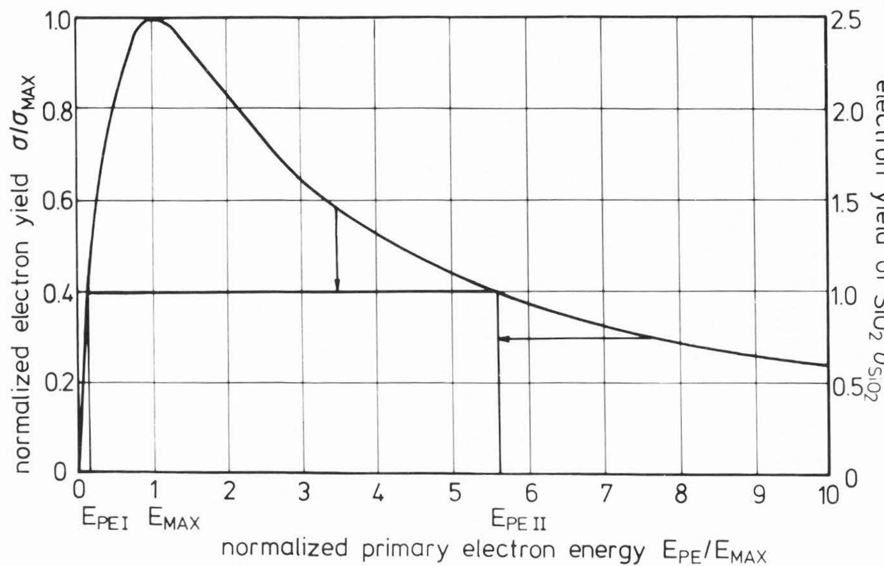

Fig. 2:
Universal electron yield curve as per Kanaya K. and Ono S. (1983). /14/, values for SiO_2 as per Seiler H. (1983). /27/; arrows indicate the mechanisms of charging at the passivation surface.

Fig. 1.1 was taken immediately after -5 V was applied to the upper row and +5 V to the lower row. Both the unpassivated and the passivated parts show the same bright or dark contrast. Whereas the voltage contrast in the unpassivated part is not a function of time, in the passivated part the CCVC decreases due to the electron radiation required for recording the image. This is shown by the micrograph taken immediately afterwards (Fig. 1.2). The contrast has completely vanished within the storage time (Fig. 1.3). If the applied voltage is switched off after the CCVC has disappeared (Fig. 1.4), then in the unpassivated part has vanished with the voltage whereas a contrast is again seen in the passivated regions, although it is inverted with respect to the previous one. This contrast also vanishes gradually with irradiation, as is shown in Figs. 1.5 and 1.6.

Observation of the turnon and turnoff of static voltage on the TV monitor shows that the CCVC vanishes the more quickly the larger the PE current and the smaller the irradiated surface. The storage time therefore depends on the current density. The contrast and the storage time are the same for turnon of a voltage and turnoff of an inverted voltage i.e., only the voltage difference ΔV is critical. The storage time T_{bright} of the bright CCVC for negative voltage differences is greater than the storage time T_{dark} of the dark CCVC for positive voltage differences (cf. Fig. 1.5, where the dark contrast has almost vanished, whereas the bright contrast is still visible!).

The fundamental precondition for the occurrence of CCVC, namely the use of PE energies lower then E_{PEII}, can be explained by the electron yield σ of the passivation layers. In this energy region, the electron yield σ , which is the sum of the secondary electron (SE) yield and the backscatter electron (BE) yield η :

$$\sigma = \delta + \eta$$

is greater than one for all usual passivation materials. The result of this, as is evident from the universal dependence of the yield on the PE energy E_{PE} shown in Fig. 2, is that the combined SE and BE currents leaving the specimen $I_{SE}+I_{BE}$ are greater than the PE current I_{PE} when $E_{PEI} \ll E_{PE} \ll E_{PEII}$. The irradiated passivation surface is thus positively charged. Low-energy SE can therefore no longer leave the surface and the SE current drops until the current of the emitted electrons is equal to that of the incident PE. The charging then no longer increases since it has reached its equilibrium state. If the PE irradiation is changed, then the charging of the passivation surface readjusts to the changed condition so that the SE and BE currents are equal to the PE current. The state of the passivation surface is therefore determined by the dynamic equilibrium between the incident and emitted currents. The small positive charge consequently acts as a potential barrier for the SE, its position being determined by the dynamic equilibrium just described which is set up for all PE energies in the region $E_{PEI} \ll E_{PE} \ll E_{PEII}$. The basic precondition for CCVC is thus an electron yield of the passivation surface greater than 1.

This critical dynamic equilibrium does not occur for larger PE energies $E_{PE} \gg E_{PEII}$. The passivation surface is negatively charged due to $\delta < 1$ until the PE have only so much energy with respect to the surface that the point E_{PEII} (Fig. 2) is reached, so that an equilibrium is now established between the currents due to the strong charging. The CCVC effect can no longer be observed with such strong charging.

These considerations relating to the dynamic equilibrium between incident and emitted currents provide an understanding of CCVC on the basis of a model which will now be examined in greater detail with reference to Figs. 3, a to d.

The positive charging taking place for $E_{PEI} < E_{PE} < E_{PEII}$ on the passivation surface in dynamic equilibrium as well as the charge additionally induced on the interconnections by switching processes are shown schematically in Fig. 3a. Fig. 3b shows the associated surface potentials at the time of switching. The hatched

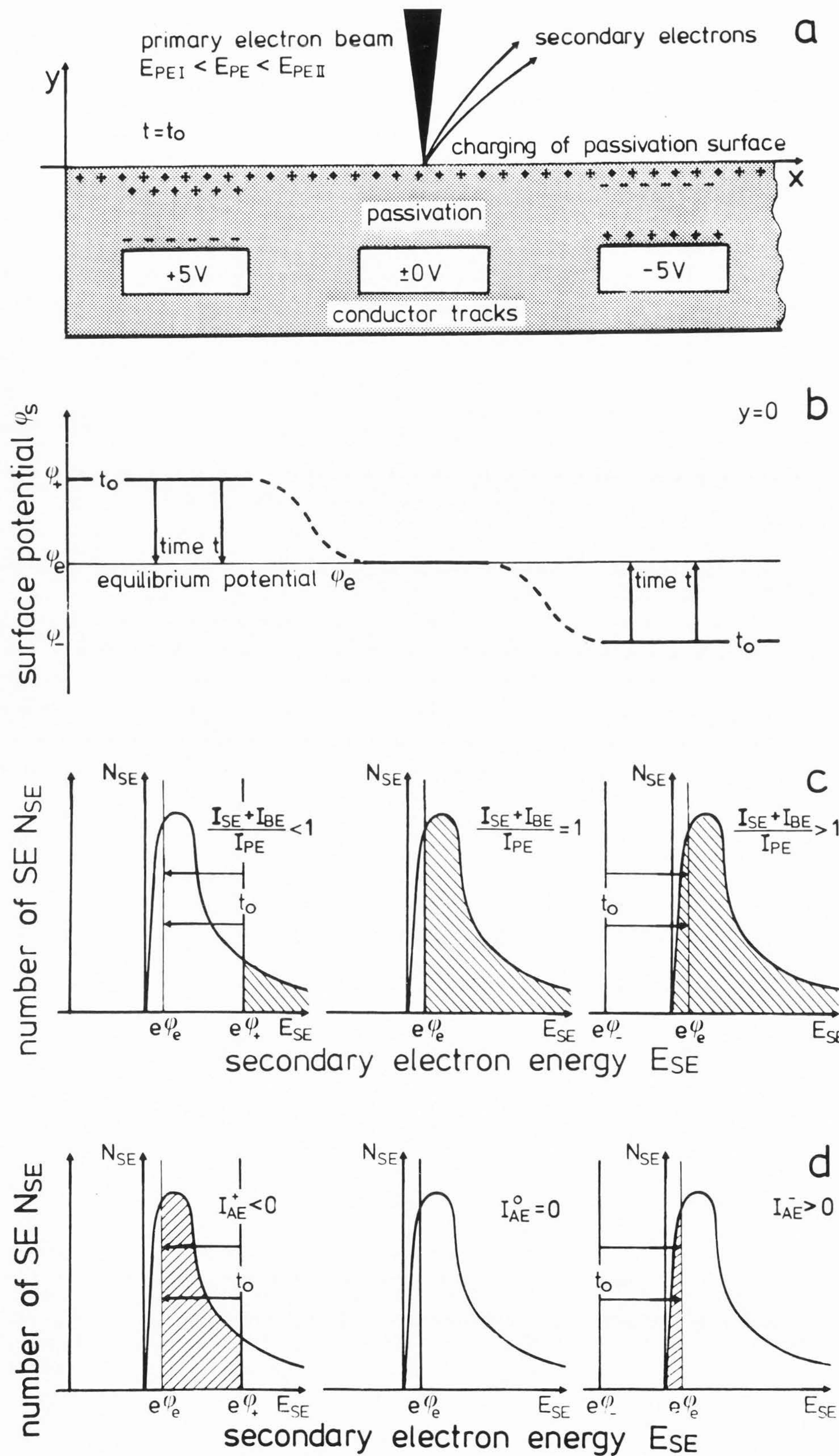

Fig. 3:
Model for the CCVC (cf. Fig.1)

a) schematic view through the surface of an IC with 3 conductor tracks; voltages of +5V, ±0V and -5V are switched on at time $t = t_o$

b) Surface potential φ_s when switching on voltages at $t = t_o$ and its charge during the irradiation time $t > t_o$

c) change of SE signal due to time dependent surface barrier $e \cdot \varphi_s(t)$

d) part of the SE spectrum representing the absorbed current I_{AE} that compensates the induced charges at the surface.

areas in the $N_{SE}(E_{SE})$ plots in Figs. 3c and d show the detected current $I_{SE} + I_{BE}$ scaled to the PE current and the absorbed current I_{AE} discharging the passivation surface, respectively.

Above an interconnection carrying a voltage of 0V, a positive charge is set up due to $\sigma > 1$ (Fig. 3a, middle track) and an associated positive equilibrium potential (Fig. 3b, middle part) arises. The current $I_{SE} + I_{BE}$ emitted from the potential barrier is in equilibrium with the incident current I_{PE}, i.e., the current absorbed by the passivation surface $I_{AE} = I_{AE}^{0}$ vanishes (Figs. 3c, d, middle diagrams). The passivation surface acquires no further charge in accordance with the processes discussed above.

If a positive voltage of +5 V is applied to the interconnection after the equilibrium state has been reached (Fig. 3a, left), then negative charges are induced locally - in a manner analogous to the processes at a capacitor dielectric - at the boundary layer to the interconnection, resulting in additional positive charges appearing at the passivation surface. The charging state of the surface changes accordingly, and the surface potential φ_s increases to the value φ_+ (Fig. 3b, left). The greater potential barrier reduces the emitted SE current (cf. Fig. 3c, left). This interconnection therefore initially appears dark against the grounded interconnection. The dynamic equilibrium between incident and emitted currents is disturbed. The current absorbed in the potential barrier I_{AE}^{+} is negative (Fig. 3d, left) and compensates the positively induced charge in the storage time T_{dark}. The surface potential φ_e has again reached the equilibrium value (Fig. 3b, left) and the CCVC vanishes.

Analogously, application of a negative voltage of -5 V results initially in an additional negative induced charge at the passivation surface (Fig. 3a, right). The surface potential assumes the smaller value φ_- (Fig. 3b, right). Since no potential barrier exists, all SE can leave the surface and a bright contrast is produced (Fig. 3c, right). The positive absorbed current I_{AE}^{-} (Fig. 3d, right) then dissipates the induced negative charge, so that within the storage time T_{bright} the surface potential φ_s reaches the equilibrium value φ_e and the contrast vanishes.

This model therefore shows that CCVC occurs within the storage time after turnon and turnoff of static potentials. This storage time should become shorter with increasing current density and its consequent quicker compensation of the induced charge. Since the value of the absorbed I_{AE}^{+} generally exceeds that of I_{AE}^{-} (cf. hatched areas in Fig. 3d), positive induced charges should be compensated more quickly than negative ones, i.e., the storage time T_{dark} is smaller than the storage time T_{bright}. This explains the experimental results obtained on the test structure (cf. Fig. 1).

Theory

The quantitative description of the CCVC effect is based on the quantitative investigation of the current which enters and leaves the passivation surface. The absorbed current I_{AE} is given by the current balance between the incident PE current I_{PE} and the emitted currents of the SE and BE, I_{SE} and I_{BE} :

$$I_{AE} = (I_{SE} + I_{BE}) - I_{PE} \qquad (1)$$

or by means of the total, secondary and backscattered electron yields σ, δ and η :

$$I_{AE} = (\sigma - 1)I_{PE} = ((\delta + \eta) - 1)I_{PE} \qquad (2)$$

The CCVC effect occurs only for those PE energies for which the total electron yield is greater than 1. Since the current of the emitted electrons exceeds that of the incident ones, the passivation surface is charged to a positive surface potential φ_s. The potential barrier which develops is approximately equal to the surface potential φ_s for small attracting field strengths (50 - 100 V/m) and especially for small structures. Since the surface potential changes in exactly the same way as the charge on the surface during irradiation, the result is an emitted SE current which varies with time :

$$I_{SE}(t) = I_{PE}\,\delta(E_{PE}) \int_{e\varphi_s(t)}^{50\,eV} N_{SE}\, dE_{SE} \cdot \left(\int_{0\,eV}^{50\,eV} N_{SE}\, dE_{SE} \right)^{-1} \qquad (3)$$

in which (E_{PE}) describes the PE energy dependence of the SE yield and $N_{SE}(E_{SE})$ the SE spectrum, i.e., N_{SE} is the number of SE in the energy interval dE_{SE}. The reduction of the SE current by the potential barrier $e\varphi_s(t)$ is calculated from the first integral, the second integral being used to standardize the spectral function N_{SE}. According to equation 2, a change of the SE current $I_{SE}(t)$ also leads to a change in the absorbed current $I_{AE}(t)$ charging the passivation surface. Consequently, the surface potential $\varphi_s(t)$ also changes. This change is determined by the capacitance of the passivation layer C_{Pass} and the integral of the charging current $I_{AE}(t)$:

$$\varphi_s(t) = \frac{1}{C_{Pass}} \int_{t_0}^{t} I_{AE}\, dt + \varphi_s(t_0) \qquad (4)$$

where the capacitance of the passivation layer :

$$C_{Pass} = \frac{\epsilon_0\, \epsilon_r\, A}{d} \qquad (5)$$

is given by the uniformly irradiated area A and the thickness d and permittivity $\epsilon_0\, \epsilon_r$ of the passivation layer, and $\varphi_s(t_0)$ is the initial surface potential at time t_0.

Within the storage time, therefore a dynamic equilibrium is established when the equilibrium potential φ_e is reached. Both the storage time

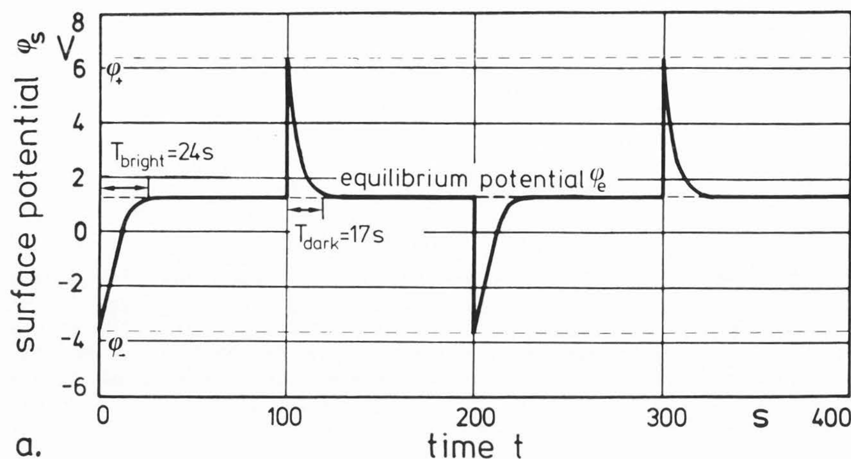

Fig. 4:
Simulation of CCVC: time dependence of current ratio (b) and surface potential (a) at a 0.36 µm SiO_2 passivation, when a voltage difference ΔV = ±5V is switched every 100 s (cf. Fig. 3d or 3b, respectively).

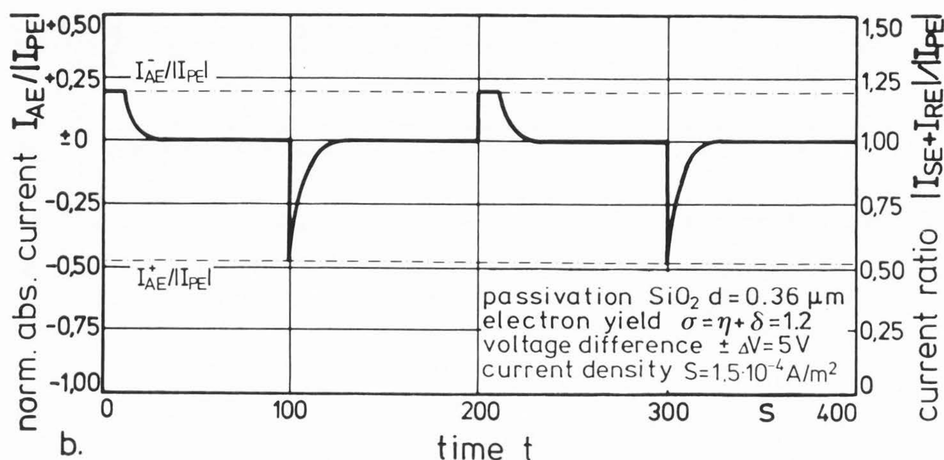

and the equilibrium potential depend on the SE spectrum $N_{SE}(E_{SE})$ and on the electron yield σ and thus on the passivation material and the PE energy.

In the following computer simulations, the SE spectrum N_{SE} was calculated in accordance with /26/:

$$N_{SE}(E_{SE}) = \frac{E_{SE}}{(E_{SE} + A)\,(E_{SE} + \Phi)^y} \qquad (6)$$

where parameters A, Φ and y assume suitable values for SiO_2. The electron yield curve used is obtained by taking into account the dependence of the SE yield $\delta(E_{PE})$ on the PE energy as per /27/:

$$\delta(E_{PE}) = \left(\frac{E_{PE}}{E_{PE\,MAX}}\right)^{-0.38} \cdot 1.11\,\delta_{MAX} \cdot$$

$$\left(1 - \exp\left(-2.3\left(\frac{E_{PE}}{E_{PE\,MAX}}\right)^{1.35}\right)\right) \qquad (7)$$

and by using a BE yield value of η = 0.18 which is approximately constant over the PE energy range, and a value of E_{PEMAX} = 300 eV for the position of the yield maximum as per /14/ for silicon oxide. This results in a value of 1150 eV for the upper limit E_{PEII} of the CCVC existence region. This value varies from specimen to specimen and is strongly dependent on the pretreatment to which the passivation surface had been subjected to /17/. It must therefore be matched to the experimental values in each case.

The time-dependence of the CCVC effect was calculated with the aid of these equations. Fig.4 shows the waveform of the surface potential (a) and of the normalized absorbed current (b), when a voltage difference ΔV = ±5 V is switched every 100 s. An SiO_2 passivation, 0.36 µm thick, an electron yield $\sigma = \eta + \delta$ = 1.2 and a PE irradiation with a current density S = $1.5 \cdot 10^{-4}$ A/m² are assumed. The waveform, which has already been described qualitatively, is now obtained quantitatively. A striking fact is that the positive absorbed current I_{AE}^- is initially constant after switching a negative voltage difference and has a value smaller than I_{AE}^+. This is caused by the limitation due to the electron yield σ. Initially, the surface potential changes linearly. The result is that T_{bright}(= 24 s) is larger than T_{dark} (= 17 s).

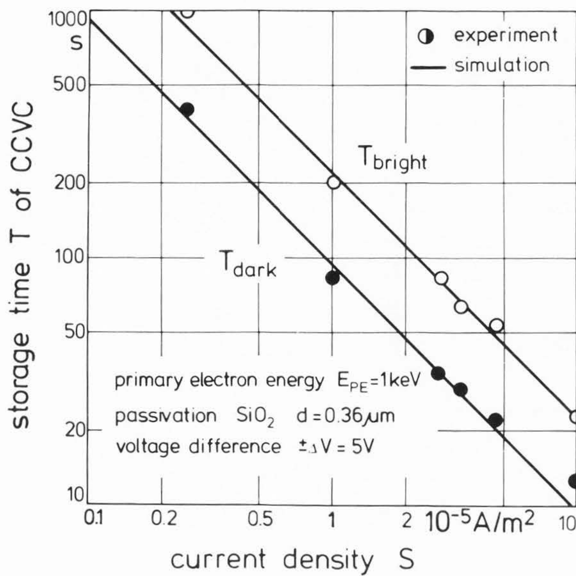

Fig. 5:
Storage times versus current density for a 0.36 μm SiO_2 passivation

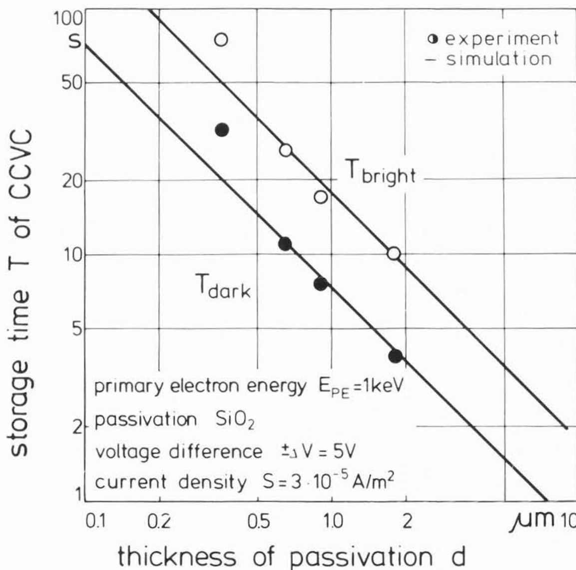

Fig. 6:
Storage times versus thickness of SiO_2 passivation.

This model and quantitative description have already been presented in /11/. A similar treatment was recently published in /32/.

Comparison of experiment and theory

The storage time is the parameter which is both typical for the CCVC effect and troublesome in its application. The experimental determination of the storage times T_{dark} and T_{bright} and their dependencies on the irradiation, passivation and signal parameters are thus necessary for utilizing this effect and are also suitable for checking the presented model and the simulation results following from it (see /13/ for more details). The following results were obtained from measurements on the test structure shown in Fig. 1.

Fig. 5 shows the experimentally obtained dependence of the storage time T_{bright} and T_{dark} on the current density S over two degrees of magnitude with a voltage swing of ± ΔV = 5 V and a PE energy of 1 keV. The passivation used is SiO_2 of a thickness d = 0.36 μm. As predicted by the model, the storage times T_{bright} are greater than T_{dark} and inversely proportional to the current density S. Similar waveforms have also been measured for other passivation layers such as Si_3N_4 and PIQ /11,13,30/. In all cases, a very good description of the experimental measuring points was obtained with the theoretically derived straight lines, in this case by using the yield σ = 1.1 in each case.

The storage times are inversely proportional to the thickness of the passivation layer. This is shown in Fig. 6 for an example of SiO_2 passivation. The slight deviation of the measuring points from the theoretical lines for thickness d = 0.36 μm can be explained by the smaller yield of the specimen used (0.36 μm SiO_2) compared with the other specimen, which also exhibited greater values for the upper boundary energy E_{PEII}.

Furthermore, the storage times become greater with increasing voltage difference. They depend by way of the permittivity ϵ_r and the yield σ of the passivation material and by way of the latter also on the primary electron energy used.

This latter dependence is also well described by the theory. Fig. 7 shows the storage times T_{bright} and T_{dark} as a function of the primary electron energy E_{PE}. The experimental values were measured only from 500 eV due to the operating range of the electron beam. They agree well with the theoretical curves which were adapted only above the boundary energy E_{PEII}. This can be determined directly by the appearance of negative charges, i.e., those showing up bright in the voltage contrast picture. The unidimensional model presented here therefore describes the CCVC effect exactly for areawise irradiation.

Predictions for electron beam testing

In the computer simulation shown in Fig. 4, the CCVC effect was investigated in a case where the passivation surface attains its equilibrium state due to the irradiation (φ_s=φ_e, I_{AE}=0), before a signal change ΔV occurs.

The aim is now to eliminate this limitation with a view to applying this effect for testing passivated devices. In the first place, the current density S is increased to a value of $2.2 \cdot 10^{-2}$ A/m². This is typical for the voltage coding technique and results from a PE current I_{PE} = $5 \cdot 10^{-10}$ A and an irradiation area of 150 μm x 150 μm /20/.

Apart from this, an initial potential $\varphi_s(t_o = 0)$ differing from the equilibrium potential φ_e is also used. This in particular permits

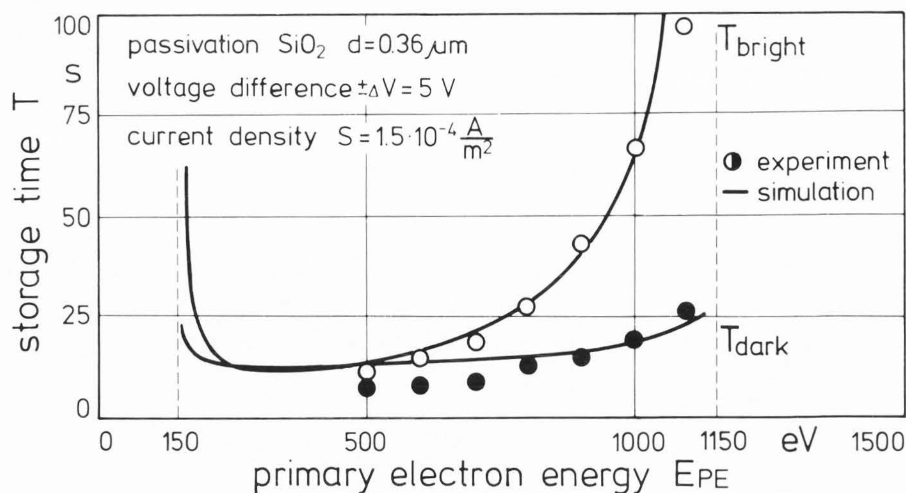

Fig. 7: Storage times versus primary electron energy for a 0.36 µm SiO_2 passivation.

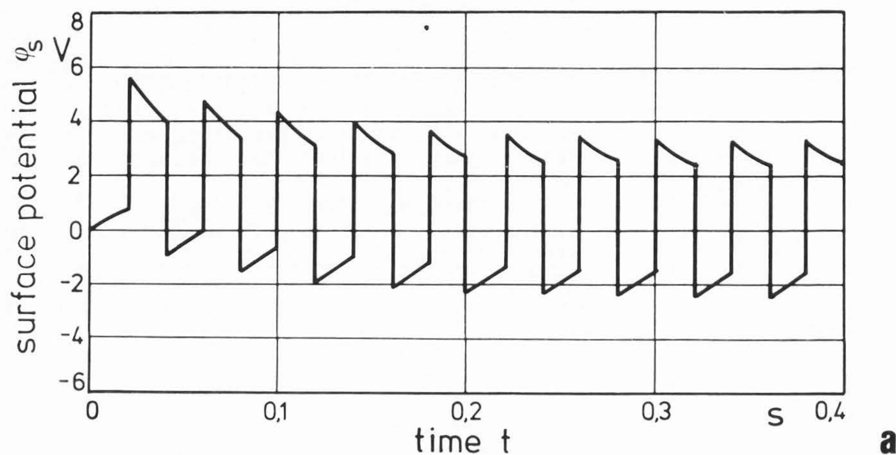

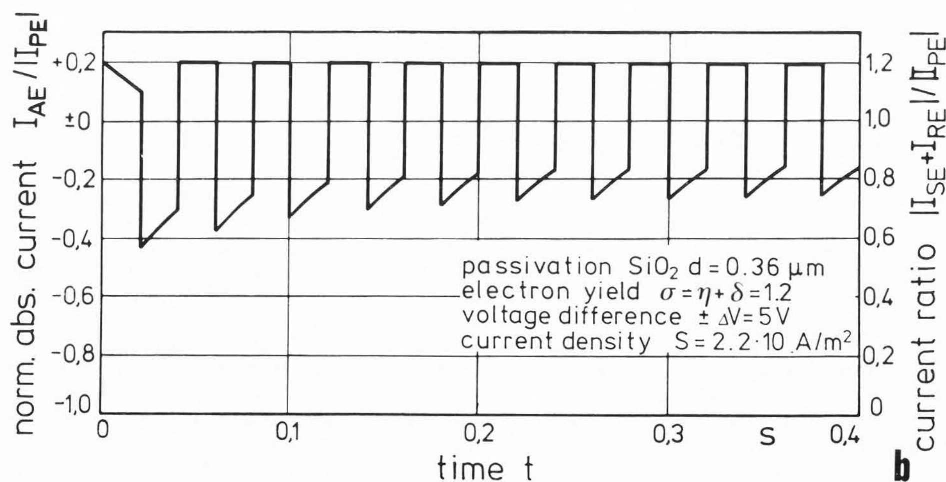

Fig. 8: Time dependence of current ratio (b) and surface potential (a); the storage times are five times the period of the square wave at the conductor track: $t_{bright} \approx t_{dark} > 5/f$.

the introduction of dc components in addition to dynamic square-wave signals. Finally, the frequency of the signals is also increased to 25 Hz.

The simulation of the surface potential is shown in Fig. 8a and that of the absorbed current in Fig. 8b.

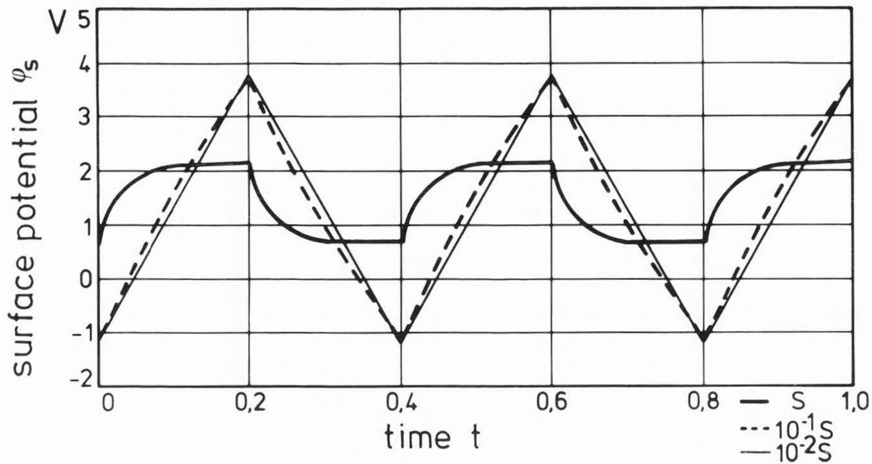

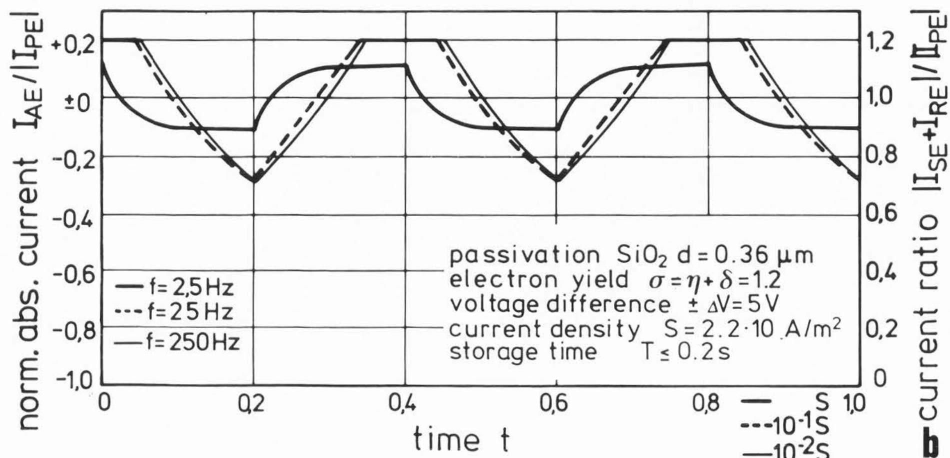

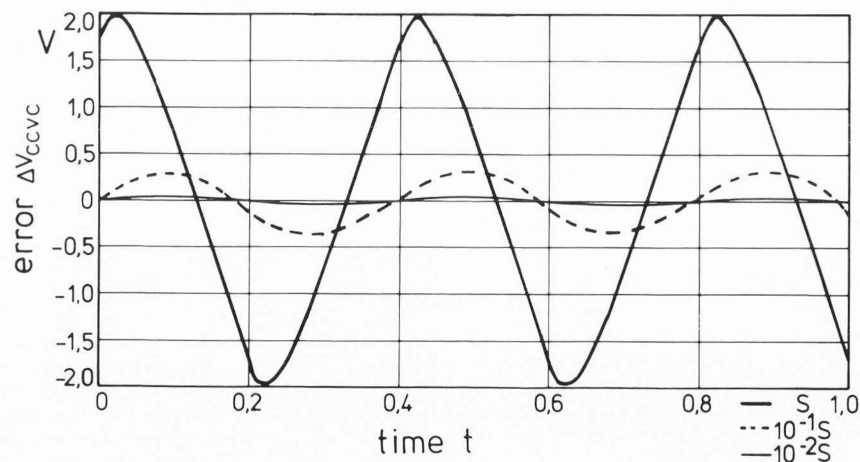

Fig. 9: Simulation of CCVC for a 5 V triangular signal and signal frequencies of 2.5Hz, 25Hz, 250 Hz with storage times of about 0.2 s: surface potential (a), current ratio (b) and error ΔV_{CCVC} caused by the effect of CCVC (c) (Note the different time scale for each signal frequency!).

Right from the start, the surface potential exhibits a tendency to assume the equilibrium value. But since the dynamic signal now has a shorter period than the storage time in each case, it is superimposed before the equilibrium potential φ_e is reached. The consequence is a surface potential waveform determined by the disappearance of the dc component within the storage times $T \leqslant 0.2$ s and the periodic switching of the square wave signal. Instead of a constant value for the square wave voltage, a slight change of up to 10% in the 5 V swing is observed in the surface potential. No totally undisturbed transfer of the dynamic signal during the CCVC is completely attained, even if the switching period for the signal change is 0.02 s, which is smaller by a factor of 10 than the storage times $T_{bright} \approx T_{dark} < 0.2$ s.

The desired undisturbed transfer of the dynamic signal to the interconnection at surface potential is, however, successfully attained at higher signal frequencies /11,13/.

The correctness of this consideration is demonstrated in Fig. 9. Under the same conditions as Fig. 8, the CCVC is here simulated for a 5 V triangular voltage at 2.5, 25 and 250 Hz. Due to the irradiation and passivation conditions, the storage times T_{bright} and T_{dark} are in this case smaller than 0.2 s. For a better comparison of the transferred signal shape, the waveforms for the current balance (b), the surface potential φ_s (a) and the error $\Delta V_{CCVC} = \Delta V_{signal} - \varphi_s$ (c) for the frequencies 25 and 250 Hz are in each case increased by a factor of 10 and 100 respectively as against the 2.5Hz plot. For 25 Hz, the signal period (T_p = 0.4 s) is almost twice as large as the storage time, the surface potential therefore deviates strongly from the triangular voltage waveform and the error exhibits values up to 2 V, i.e., the relative error is 40%. For a frequency f = 25 Hz, the waveform of the surface potential deviates only minimally from the original triangular shape of the voltage signal. In the ratio $T_p/T_{dark} = 0.2$, the relative error $\Delta V_{CCVC}/\Delta V < 0.4V/5V = 8\%$ and finally for a frequency of 250 Hz with a ratio $T_p/T_{dark} = 0.02$, the relative error $\Delta V_{CCVC}/\Delta V < 0.04V/5V = 0.8\%$. Within the scope of the accuracy attainable in electron beam testing therefore, and for such small ratios of signal period to storage time, a practically error-free quantitative voltage measurement is assured using the CCVC effect.

When using a smaller storage time T_{dark}, a value of $\Delta V_{CCVC}/\Delta V$ is obtained for the relative error due to the CCVC effect at a signal swing ΔV:

$$\frac{\Delta V_{CCVC}}{\Delta V} \leqslant \frac{T_p}{T_{dark}} \qquad (8)$$

where T_p is the period of the periodic signal.

Within the scope of the simulation, this estimate is valid only for test techniques with areawise irradiation and unpulsed electron beams. It may, however, also be applied to other test methods.

To summarize therefore, this model permits the following predictions:

- After turnon, static signals can be detected only briefly within the storage time. This is inversely proportional to the current density of the electron irradiation and increases for energies close to the limiting energy E_{PEII}.
- Dynamic signals are measurable, when their temporal change is quicker than the storage time. The error due to the CCVC effect may be estimated from the ratio of signal period to storage time.

The electron beam parameters should be suitably selected for electron beam testing and the test methods should be correspondingly modified.

Application of the CCVC effect

The applications of CCVC are limited by the energy range of its appearance below E_{PEII} and by its storage time. The modifications of the test system and techniques are described and their efficiency demonstrated on the basis of examples.

Electron beam test system

The electron beam system used here is essentially the one presented in /19/. It is based on the electronoptical column of an SEM (Cambridge Instruments S 180), but has been modified to become an efficient VLSI electron beam test system by making changes in the electron gun and redesigning the electron beam chopping system, the spectrometer, the specimen chamber, the vacuum system and the IC positioning as well as by adapting various units in the measurement and control electronics and automating them by a process computer. The new design is shown in the block diagram (Fig. 10). The following important changes were made in comparison to the system described in /19/:

- Extension of the energy range for the electron probe down to 350 eV /13/
- Use of a secondary electron spectrometer of the Feuerbaum type /5/
- Automation of special functions such as specimen or beam positioning by microprocessor units /10,13/
- Incorporation of the vector scan unit (VSU) and window scan unit (WSU) for testing passivated components with a high-energy electron beam /10,13/
- Incorporation of a new, fast digital image acquisition system (FDIAS) /13,24/
- Incorporation of a new multisampling system (MSS) /1,13/.

The last two improvements are of special importance for electron beam testing, using the CCVC effect. There is no point in going into the details of FDIAS and MSS design (see /24/ or /1/ for these), but their function is explained on the basis of the subsequent diagrams.

FDIAS permits a voltage contrast micrograph to be recorded and stored by way of a digital scan with a maximum point frequency of 10 MHz. The spatial resolution may be selected from 128 x 128 to 1024 x 1024 pixels. The information depth per point (1 bit in the diagrams) is designed for 8 bits. The main requirement in the development of this system was, in contrast to similar systems /7,25/, a high recording speed. The aim was to allow recording of CCVC images at high magnification (i.e., short storage time). FDIAS permits an image with 1024 x 1024 pixels to be recorded and stored in 0.3 s. The record-

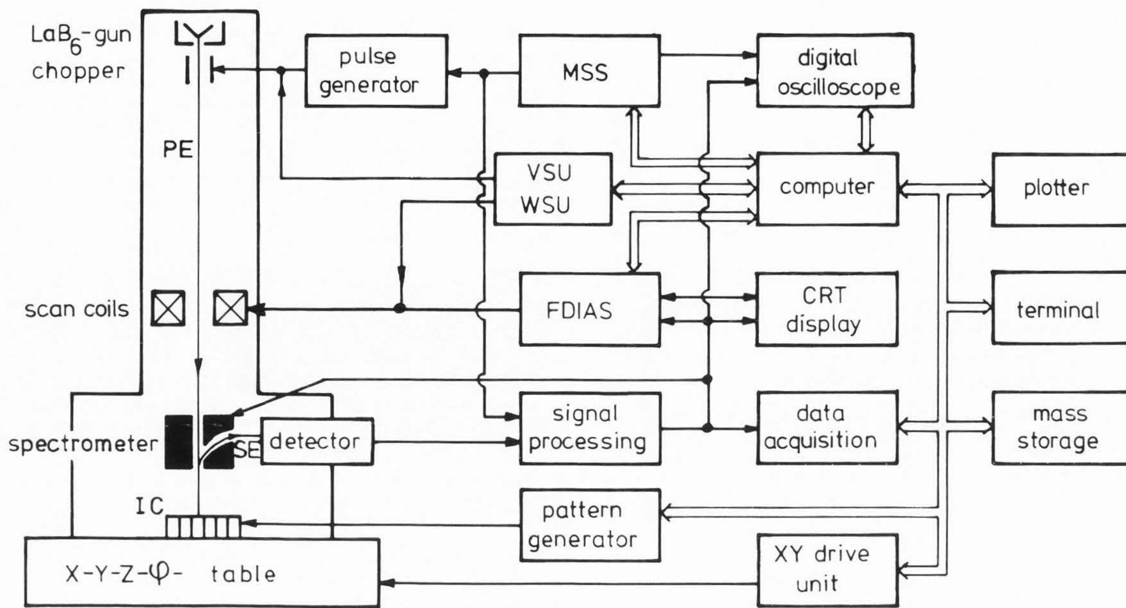

Fig. 10: Block diagram of the electron beam test system.

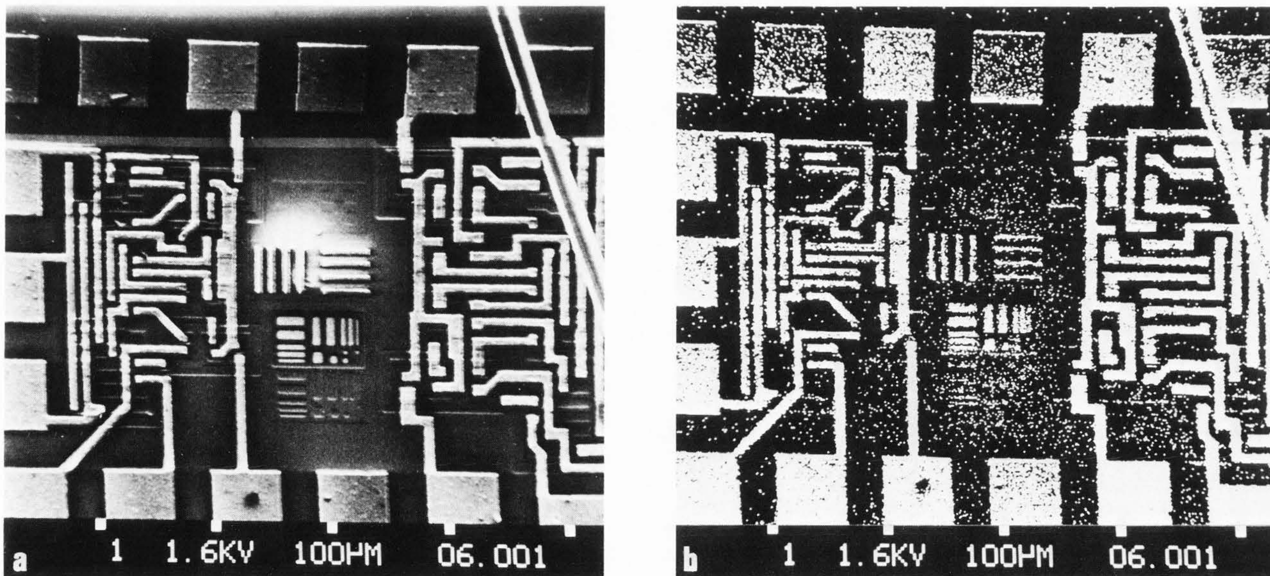

Fig. 11: Comparison of standard and new fast digital image acquisition system (FDIAS /24/) :
standard (a): 800 lines, 60 s exposure time
digital (b): 1024 x 1024 pixels, 15.2 s recording time.

ing quality of a standard SEM image (800 lines in 60 s) is compared in Fig. 11 with an FDIAS image (1024 x 1024 pixels in 15.2 s).

The voltage of high-frequency periodic IC-internal signal waveforms can be measured by means of voltage contrast with the aid of the sampling principle /5,20/. A usable result does, however, presuppose a sufficient signal-to-noise ratio. This can be achieved in conventional sampling systems by scanning the signal repeatedly prior to every phase change, thus reducing the noise component. The number of scans at constant phase is designated as N_{PH}. After N_S phase changes, the desired signal waveform is measured. The irradiation time is therefore calculated from:

$$T_{IR} = N_{PH} \cdot N_S \cdot t_p, \quad (9)$$

where t_p is the duration of the electron pulse. In quantitative voltage determination by means of CCVC, the use of this method involves a measure-

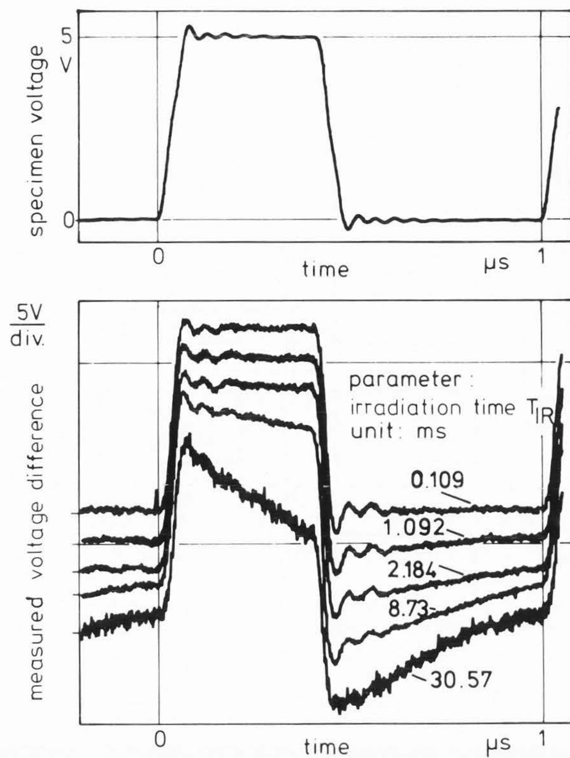

Fig. 12:
Quantitative waveform measurement via CCVC by use of the multisampling (MSS /1/) : dependence on the sampling time T_{SA} (e-beam parameters : energy = 1.3 keV, current I_{PE} = 0.7 nA, pulse width t_p = 10 ns, duty cycle c = 10^{-2} scanned over an area A = $4.2 \cdot 10^{-9} m^2$ of a SiO_2 passivated pad, d = 1.8 µm.

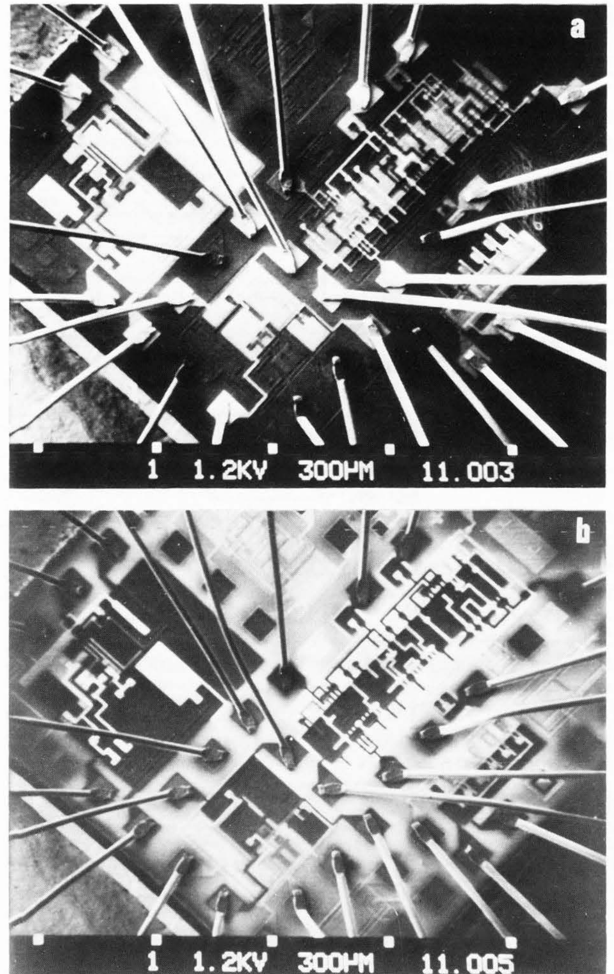

Fig. 13:
CCVC-picture of a CMOS-circuit with static voltages using the standard setup for low magnification (<20x): static signals switched on (a) or off (b) (passivation SiO_2 d = 0.8 µm, beam energy E_{PE} = 1.2 kev, beam current I_{PE} = 1 nA exposure with 800 lines in 15 s).

ment error since the resulting irradiation time T_{IR} for a sufficiently good signal-to-noise ratio is too long in comparison with the prevailing storage times /1,24/.

This problem can be solved with the aid of a multisampling system (MSS), which uses very low N_{PH} values so that T_{IR} is shortened and at the same time produces a sufficiently good signal-to-noise ratio (cf. also /29/) by repeatedly recording and averaging the entire signal waveform. The irradiation time can be reduced by shortening the duration of the electron pulse t_p, which at the same time leads to an improved time resolution but impairs the signal-to-noise ratio. This is compensated in MSS by the use of a sample and hold circuit which retains the scanned signal value until the following scan and thus amplifies the signal /15/.

MSS also permits variation of the number of scans at constant phase N_{PH} and thus determination of the effect of the irradiation time on the measurement. Fig. 12 shows a square-wave IC-internal signal of period T = 1 µs and the signal waveforms measured by MSS for irradiations times of T_{IR} = 0.109 µs, 1.092 µs, 2.184 µs, 8.73 ms, 30.57 ms and values of N_{PH} = 70, 700, 1400, 5600 and 19,600 at t_p = 10 ns and N_S = 156. N_{PH} = 70 is then obtained from the ratio of the minimum settable value of the phase modification time (70 µs) and the periodic duration T = 1 µs. A primary electron current density of $9.3 \cdot 10^{-2} A/m^2$ is used, so that storage times T_{dark} = 24 ms and T_{bright} = 56 ms are obtained with a primary electron energy of 1.3 keV and an SiO_2 passivation thickness of 1.8 µm. For T_{IR} = 109 µs << T_{dark}, T_{bright} (upper curve) the CCVC has no effect on the measurement, but this effect becomes increasingly apparent for longer T_{IR} values corresponding to measurements with a conventional sampling system. The number of averaged signal waveforms is N_A = 100 in the case of T_{IR} = 30.57 ms, and 1000 for all other cases, this being reflected in the signal-to-noise ratio.

Examples and efficiency

Static signals can be detected via CCVC in passivated devices after turnon only within the storage time. For small magnifications, i.e., for

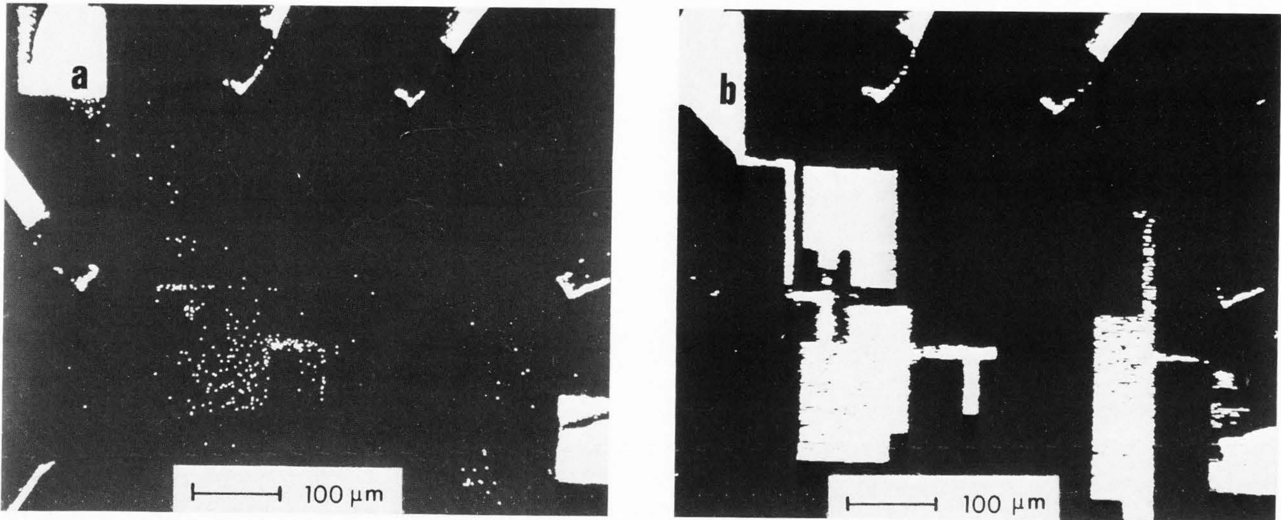

Fig. 14: CCVC-picture of a CMOS operational amplifier with static voltages using FDIAS for higher magnifications (> 200x)
acquisition time 4.1 s or 3.2 µs per point (a)
0.26 s or 0.2 µs per point (b)
(passivation SiO_2 d = 0.8 µm, beam energy E_{PE} = 1.5 keV, beam current I_{PE} = 1 nA, resolution: 1024 x 1024 pixels).

small current densities of the electron irradiation, this can be effected without difficulty with a standard SEM and by using primary energies immediately below E_{PEII}. This is demonstrated in Fig. 13; after turnon of the static voltage, the same image is obtained as for an unpassivated device (a) (cf. Fig. 1.1), whereas after turnoff an inverted contrast image is obtained (b) (cf. Fig. 1.4).

For high magnifications, the storage time is reduced with increasing current density so that rapid image recording is necessary. This is shown in Fig. 14. Only with a very short image recording time of 0.26 s (or 0.2 µs per image dot), can the applied static voltages be detected by means of CCVC (b). With a time 16 times as long, the CCVC is dissipated by excessive irradiation and no contrast can be detected in the passivated areas (a).

Test methods with areawise scanning of larger specimen regions with information displayed in the form of a micrograph and subsequent image evaluation are particularly suitable for utilizing the CCVC effect /18,33/. In such methods, the requirement that the signal period has to be smaller than the storage time is easily met. In the low-frequency range from about 1 Hz to 2 MHz this can be done by voltage coding /20/. Fig. 15 shows the characteristic bright-dark pattern of the clock signals Φ_1, and Φ_2 on an 8085 microprocessor passivated with 0.8 µm Si_3N_4 and demonstrates the spatial resolution attainable with CCVC on 2 µm wide interconnections. Stroboscopic voltage coding (also known as phase stepping /30/) is a suitable method for high-frequency signals. It is to be preferred to

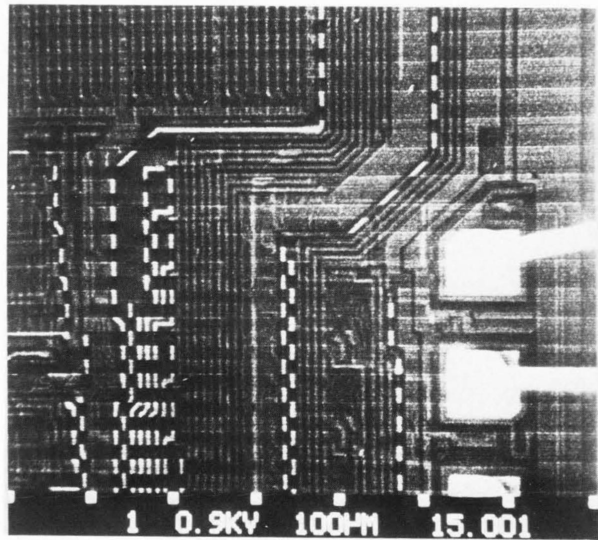

Fig. 15:
Voltage coding micrograph of an 8085-microprocessor showing the clock signals $\emptyset_1$ and $\emptyset_2$ (frequency f = 200 KHz, passivation Si_3N_4 d = 0.8 µm, beam energy E_{PE} = 0.9 keV, beam current I_{PE} = $5 \cdot 10^{-10}$A).

logic state mapping /23/ since it irradiates a greater area and not just a single line so that a greater storage time is obtained with smaller current density, as explained in /30/. These test methods allow direct logic analysis and also, with use of computer-controlled image recording and evaluation system, semi-quantitative voltage determination /18,25/.

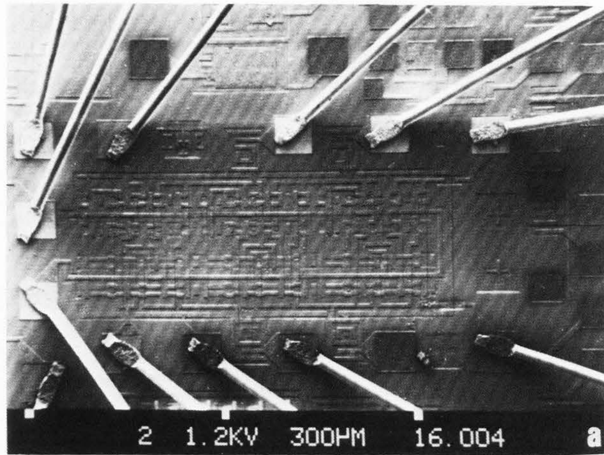

Fig. 16:
Frequency tracing at a CMOS frequency divider, input frequency 50 kHz;
SEM-image without voltage applied (a)
trace frequency f = 50 kHz (b)
f/2 = 25 kHz (c)
f/4 = 12.5 kHz (d)
f/8 = 6.25kHz (e)

(passivation SiO_2 d = 0.8 µm, beam energy E_{PE} = 1.2 keV; beam current I_{PE} = 2 nA.

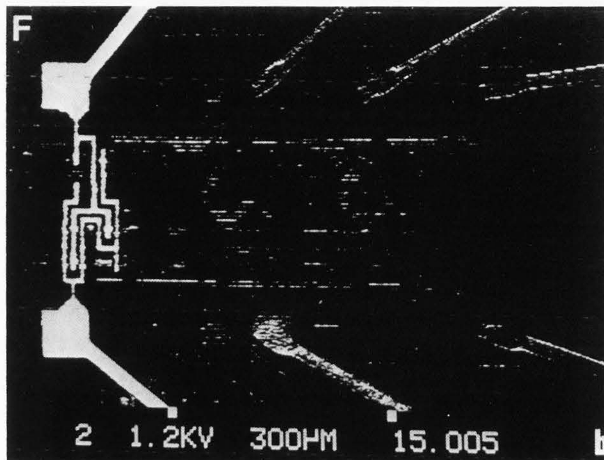

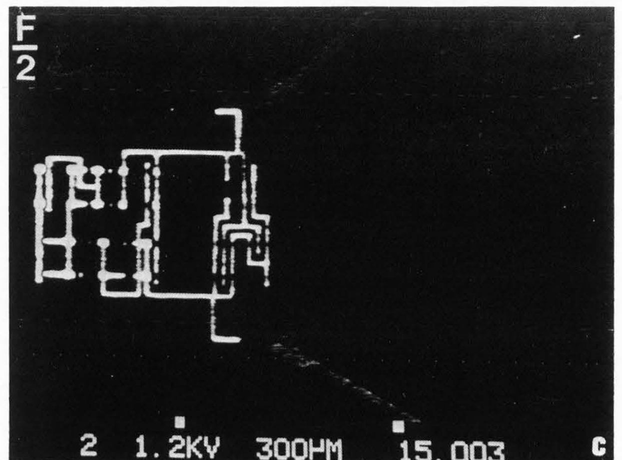

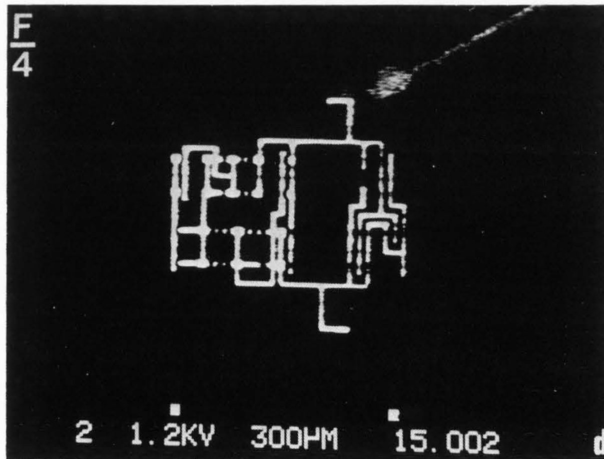

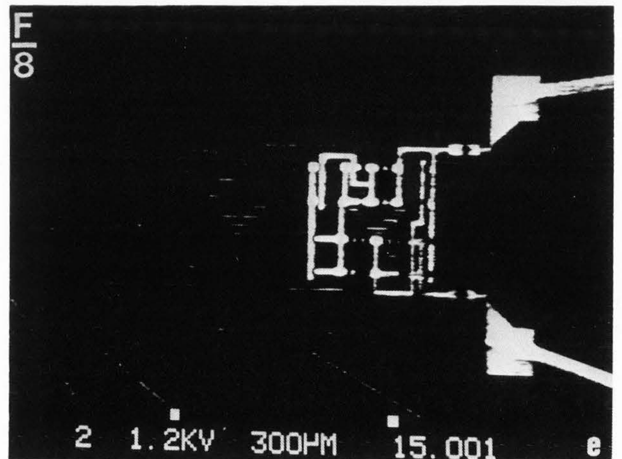

The use of the frequency tracing test method /2/ with the aid of CCVC can be seen in Fig. 16. Diagram (a) shows the device - a CMOS frequency divider - in an SE image without voltage signals. Depending upon the detection frequency set, only those structures are visible in (b) which carry the device input frequency f. Diagrams (c), (d) and (e) show the corresponding structures for the divided frequencies f/2, f/4 and f/8. It is clear that similar structures were used in each stage of the frequency divider. The frequency mapping method, operating on the same detection principle, can be applied in a similar way /2/.

The use of CCVC test methods with permanent-positioned electron beams involves greater problems since the high current density means short storage times and the use of high beam currents I_{PE} to improve the voltage resolution V_{min} in line with the Gopinath formula /8/:

$$V_{min} = n \cdot C \sqrt{\frac{\Delta f}{I_{PE}}} \qquad (10)$$

where n is the signal-to-noise ratio C the spectrometer constant and Δf the bandwidth of the detection system. If a sufficiently long storage time cannot be set despite selection of a primary energy just below E_{PE} and, if necessary, scanning other electron beam over an area or along a line, then the primary current must be reduced at the expense of the voltage resolution. The signal-to-noise ratio can then be improved by averaging repeated measurements (cf. MSS).

A spectrometer must be used for quantitative measurements with linearization and for improving the signal-to-noise ratio in logic analysis. The measuring errors arising in this process due to micro field effects /22/ are minimized by high attracting fields and suitable selection of the operating point of the barrier voltage V_B /20,22/. When using the CCVC effect, however, high attracting fields cannot be used since they cancel the microfields and the potential barrier and thus disturb the dynamic equilibrium between incident and emitted currents which is critical for this effect. Thus local charges occur with high attracting fields and permanently a positioned beam, and these prevent voltage measurement. The use of low homogeneous attracting fields between 50 and 100 V/mm and an increased barrier voltage $V_B > 3$ V has proved to be a suitable compromise.

CCVC cannot be used for quantitative real-time voltage measurements since the bandwidth of the linearization circuit is about 100 kHz and the storage times are smaller than 10 µs for a permanently positioned beam and the requisite high currents. A real-time logic analysis is, however, possible in the region above about 100 kHz up to the detection limit (about 10 MHz) /23,31/.

An example of a quantitative signal waveform measurement with MSS on a 5-µm wide interconnection passivated with 0.9 µm SiO_2 is shown in Fig. 17. Due to the reduced irradiation time T_{IR} = 59.1 µs for a measurement over the entire periodic signal waveform, the CCVC effect causes no deformation (cf. Figs. 8,9). The desired signal-to-noise ratio was obtained by averaging 100 measurements.

The voltage resolution attainable with CCVC is, in principle, not limited by the CCVC effect itself but is, just like measurements on unpassivated devices, determined by the signal-to-noise ratio, the quality of the detection system and the beam current in accordance with the Gopinath formula /8/.

To determine the voltage resolution with the aid of the CCVC effect, an amplitude-modulated specimen signal was used. This was a high-frequency carrier signal which is detectable without impairment during the CCVC effect and the actual wanted signal, which may be selected to have low frequency. With the aid of a lock-in amplifier, the low-frequency wanted signal can now be demodulated from the detected SE signal and thus be measured. Fig. 18 shows a wanted signal with an amplitude of 7 mV measured by this procedure. The attainable voltage resolution thus lies in the same order of magnitude as for measurements made on unpassivated devices /19,21/.

The attainable time resolution is also identical with that obtained from unpassivated devices. Since the passivation layers used in the frequency area of interest show no dielectric losses up to some GHz, the time resolution in this case is also given by the electron beam pulse used. A low-frequency limitation naturally exists during the CCVC storage time.

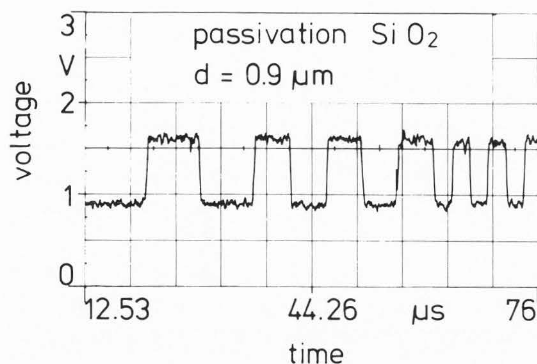

Fig. 17:
Waveform measurement using MSS at a conductor track, 5µm wide. (passivation SiO_2 d=0.9µm, beam energy E_{PE}=1.3keV, beam current I_{PE}=2nA, pulse width t_p=50ns duty, cycle $c=5\cdot10^{-4}$, sampling time t_{SA}=32ms, number of averages N_A=100).

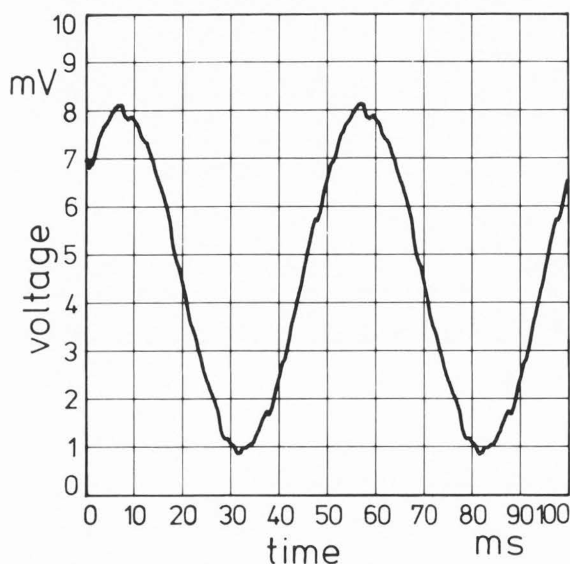

Fig. 18:
Demonstration of a voltage resolution of 7mV via the CCVC (passivation SiO_2 d=0.64µm, beam energy E_{PE}=1.2keV, beam current I_{PE}=50nA.)

The attainable spatial resolution is, as with unpassivated devices, determined by the focusing of the electron beam and particularly by the beam current. Apart from this, however, the micro field produces an inhomogeneous field profile within the passivation so that the induced charge distribution on the passivation surface does not correspond to that of the interconnection. The result is therefore an expansion compared with the interconnection lying beneath this surface. This effect becomes serious when the

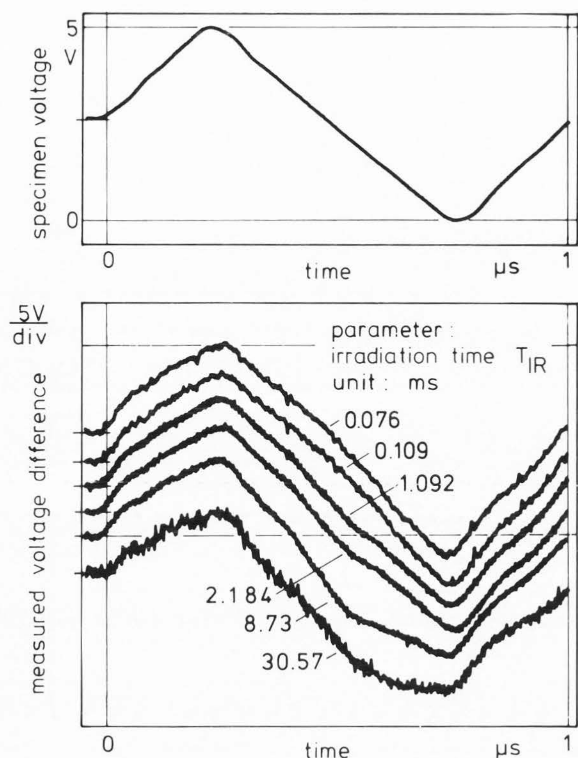

Fig. 19:
Quantitative waveform measurement of a triangular signal demonstrating linearity for quick sampling (passivation SiO_2 d = 1.8 μm, beam energy E_{PE} = 1.3 keV, beam current I_{PE} = 0.7 nA, pulsewidth t_p = 50 ns, duty cycle c = 10^{-2}, number of averages N_A = 1000 (N_A = 100 for lower curve!).

spacing between two adjacent interconnections is smaller than the thickness of the passivation layer lying above it. The design must therefore include "test pads" for quantitative voltage measurement, as for unpassivated circuits (due to the microfield effect) /34/.

The linearity obtained in the quantitative voltage measurement with MSS is demonstrated in Fig. 19. With short irradiation times T_{IR}, the triangular signal is measured exactly. Not until T_{IR} attains the same order of magnitude as the storage times does the CCVC effect lead to distortion. The figure shows that CCVC can be used to obtain an exact quantitative voltage measurement of IC-internal signals.

Conclusion

The CCVC effect occurring at low PE energies permits direct nondestructive electron beam testing of passivated devices. However, limitations arise in its use due to the CCVC effect itself. The critical parameter here is the storage time, the time within which CCVC is dissipated by electron irradiation after application of a voltage. It is inversely proportional to the current density and the passivation thickness, increasing with the voltage value applied, is smaller for positive voltage swings than for negative ones and depends on the type of passivation and the PE energy used. By considering the currents occurring on the passivation surface, a computer simulation was used to obtain a quantitative description of this effect as well as the dependencies of the storage time. The consequences for applications are that both logic states and static voltages can be detected only after being turned on within the storage time, and dynamic signals can be measured only when their period is shorter than the storage time. This means that for sampling measurements the decisive irradiation time T_{IR} must be shorter than the storage time. If this is taken into account by suitably selecting the irradiation parameters or by modifying the electron beam test techniques (cf. FDIAS, MSS), then passivated IC can be successfully tested by electron beams where the spatial, time and voltage resolution are known (as was shown in the examples).

Acknowledgements

The authors would like to thank the Federal Ministry of Research and Technology (BMFT) and the Minister of Science and Research of North-Rhine Westphalia for their financial support.

References

1 Bourquardez M, Reiners W, Herrmann KD, Görlich S, Kubalek E. (1986). Improvement of electron beam waveform measurement at passivated VLSI devices by application of the multi-sampling-method. Scanning, in press.

2 Brust H-D, Fox F, Wolfgang E. (1985). Frequency tracing and mapping: Novel electron beam testing methods. in: Proc. Int. Conf. Microlithography: Microcircuit Engineering 84, Berlin, Heuberger A, Beneking H (eds), Academic Press London, 411 - 425

3 Crosthwait DL, Ivy FW. (1974). Voltage contrast methods for semiconductor device failure analysis. Scanning Electron Microsc. 1974: 935 - 940.

4 Fazekas P, Fox F, Papp A, Widulla F, Wolfgang E. (1983). Electron beam measurements in practice. Scanning Electron Microsc. 1983; IV: 1595 - 1604.

5 Feuerbaum HP. (1979). VLSI testing using the electron probe. Scanning Electron Microsc. 1979;I: 285 - 296.

6 Fujioka H, Nakamae K, Ura K. (1980) Function testing of bipolar IC's and LSI's with the stroboscopic scanning electron microscope. IEEE Solid State Circuits, SC-15, 177 - 183.

7 Fujioka H, Tsujitake M, Ura K. (1982). Voltage contrast isolation by frame-by-frame subtraction in the scanning electron microscope. Scanning Electron Microsc. 1982; III: 1053 - 1060.

8 Gopinath A. (1977). Estimate of minimum measurable voltage in the SEM. J.Phys.E: Sci.Instr. 10, 911 - 913.

9 Görlich S, Menzel E, Kubalek E. (1982). Capacitive coupling voltage contrast. in: Beiträge zur elektronenmikroskopischen Direktabbildung von Oberflächen, BEDO, 15, 133 - 142.

10 Görlich S, Postulka E, Kubalek E. (1983) Window scan mode for testing passivated MOS-devices. in: Microcircuit Engineering, Proc. Int. Conf. Microlithography, Cambridge, Ahmed H, Cleaver JRA, Jones GAC (eds), Academic Press, London, 493 - 500.

11 Görlich S, Herrmann KD, Kubalek E. (1984). Basic investigations of capacitive coupling voltage contrast. in: Microcircuit Engineering, Proc. Int. Conf. Microlithography, Berlin, Academic Press, London, 451 - 460.

12 Görlich S, Kubalek E. (1985). Electron beam induced damage on passivated metal oxide semiconductor devices. Scanning Electron Microsc. 1985; I: 87 - 95.

13 Görlich S. (1986). Electron beam testing of passivated integrated MOS-circuits. thesis at the University of Duisburg.

14 Kanaya K, Ono S. (1983). Interaction of electron beam with the target in scanning electron microscope. in: Electron Beam Interaction With Solids, D.F. Kyser, H. Niedrig, D.E. Newbury, R. Shimizu (eds). SEM Inc., Chicago, Il., 69 - 98.

15 Koellen DS, Brizel KW. (1983). Improved signal to noise ratio with sample and hold in the voltage contrast mode using a scanning electron microscope. Scanning Electron Microsc. 1983; IV: 1605 - 1609.

16 Kotorman L. (1980). Non-charging electron beam pulse prober on FET wafers. Scanning Electron Microsc. 1980; IV: 77 - 84.

17 Le Gressus G, Vigouroux JP, Duraud JP, Boiziau C, Geller J. (1984). Charge neutralization on insulators by electron bombardment. Scanning Electron Microsc. 1984; I: 41 - 48.

18 May TC, Scott GL, Meieran ES, Winer P, Rao VR. (1984). Dynamic fault imaging of VLSI random logic devices. IEEE/IPRS, 1, 95 - 108.

19 Menzel E, Kubalek E. (1979). Electron beam test system for VLSI circuit inspection. Scanning Electron Microsc. 1979; I: 297 - 304.

20 Menzel E, Kubalek E. (1981). Electron beam test techniques for integrated circuits. Scanning Electron Microsc. 1981; I: 305 - 322.

21 Miyoshi M, Ishikawa M, Okumura K. (1982). Effects of electron beam testing on the short channel metal oxide semiconductor characteristics. Scanning Electron Microsc. 1982; IV: 1507 - 1514.

22 Nakamae K, Fujioka H, Ura K. (1981). Local field effects on voltage contrast in the scanning electron microscope. J. Phys. D. Appl. Phys., 14, 1939 - 1960.

23 Ostrow M, Menzel E, Postulka E, Görlich S, Kubalek E. (1982). IC-internal electron beam logic state analysis. Scanning Electron Microsc. 1982; II; 563 - 572.

24 Reiners W, Herrmann KD, Kubalek E. (1986). Electron beam testing of passivated devices. in: Microcircuit Engineering, Proc. Int. Conf. Microlithography, Interlaken, in press.

25 Sardo A, Vanzi M. (1984). Digital beam control for fast differential voltage contrast. Scanning 6, 122 - 127.

26 Seah MP (1969). Slow electron scattering from metals. Surface Science 17, 132 - 160.

27 Seiler H. (1983). Secondary electron emission. in: Electron Beam Interaction With Solids, D.F. Kyser, H. Niedrig, D.E. Newbury, R. Shimizu (eds). SEM Inc., Chicago Il, 33 - 42.

28 Taylor DM. (1978). The effect of passivation on the observation of voltage contrast in the scanning electron microscope. J. Phys. D.: Appl. Physd., 11, 2443 - 2454.

29 Todokoro H, Fukuhara S, Komoda T. (1983). Stroboscopic scanning electron microscope with 1 keV electrons. Scanning Electron Microsc. 1983; II: 561 - 568.

30 Ura K, Fujioka H, Nakamae K, Ishisaka M. (1982). Stroboscopic observation of passivated microprocessor chips by scanning electron microscopy. Scanning Electron Microsc. 1982; III: 1061 - 1068.

31 Walter MJ, Eldering CA, Krevis KM, Haberer IR. (1982). Internal node testing by tester aided voltage contrast. in: Proceedings of ISTFA 1982, International Symposium for Testing and Failure Analysis, Torrance, CA, U.S.A., 156 - 161.

32 Watanabe Y, Fukuda Y, Jinno T. (1985). Analysis of capacitive voltage contrast. in: Scanning Electron Microscopy. Jap. J. Appl. Phys. 24, 1294 - 1297.

33 Younkin D. (1981). Phase dependent voltage contrast - An inexpensive SEM addition for LSI failure analysis. 19th Ann. Proc. Reliability Physics, IEEE, 1984, 264 - 268.

34 Yuasa H, Fujita M, Manabe N. (1980). SEM-Stroboscopic techniques - Their application to failure Analysis of LSI's. in: Proceedings of ISTFA 1980. International Symposium for Testing and Failure Analysis, Torrance, CA, U.S.A., 9 - 14.

Discussion with Reviewers

A.R. Dinnis: The simulation studies are presumably based on a model of the specimen which extends to infinity in the x-y plane of the specimen, so that there are no transverse fields above the specimen and the transverse distance travelled by any secondary returning to the surface is immaterial. Does the model also assume that all electrode structures in the neighbourhood of the specimen are at zero potential, or are they at a small positive potential?

K. Ura: Is the model of simulation and experiments Fig. 1 ? Please show me the assumed size of the electrode.

Authors: The comparison of simulation and experiment in Figs. 5,6,7 are based on experiments

at the test structures shown in Fig.1, having pads of 100 μm x 100 μm with different passivation layers. The simulations are strictly based on theory described in the paper, i.e., it is a unidimensional model for areawise irradiation that does not take into account the geometrical structure of the device and therefore does not deal with problems like micro field effects or local charging due to point probing. The model assumes that the passivation surface (without additional induced charging due to voltages switched at neighbouring conductor tracks) is at the equilibrium potential, i.e., at a small positive potential from 0 V to +10 V, which is determined by the electron yield and the extraction field. However, this simple model is also successfully used for understanding the other test techniques as shown in the applications.

K. Ura: The storage time may depend on the scan mode. How much is the charge deposit per one scan in the experiment? And how is it assumed in the simulation?

Authors: The influence of the scan mode on the storage time was not considered in the simulation. However, to minimize the experimental error the experiments were performed with storage times from 5 s to 1000 s being much longer than the frame repetition time of 0.5 s.

A.R. Dinnis: Have you simulated, or carried out measurements, in situations where there is an exposed conductor (e.g. a bond pad) at a positive voltage in the vicinity of the point being probed? Our results show that this can influence the equilibrium potential of the insulator surface quite significantly.

Authors: We performed experiments on the test-structure (Fig. 1) with the nonpassivated pads at positive and negative voltages (-5 V) and did not find significant differences on the storage times for areawise irradiation. Point probing was used for quantitative waveform measurements. Again we did not find an influence on the measurements using the MSS. However, in this case the unpassivated pads were at a distance of about 300 μm or more.

A.R. Dinnis: As you mention, some loss in spatial resolution is to be expected for conductors of the order of a micron in width covered with insulator of typical thickness. There will also be significant transverse fields within the insulator and above it. Have you carried out any investigations in such a situation?

Authors: The problem of spatial resolution was only shortly discussed in the paper, as it is not possible to consider them in the unidimensional model described here. More advanced simulations will deal with this problem. (They are performed by one of the authors, Mr. Herrmann, and will hopefully soon be published).

J. Reimer: You refer to an upper energy level dependence of the primary beam on the passivation manufacturing process and also the substrate surface condition. What direct influence do the passivation manufacturing process and the substrate surface condition have on the value E_{PEII}? Please explain.

Authors: The secondary electron yield and the crossover energy E_{PEII} changes due to different conditions of the passivation surface (e.g. workfunction, contamination, surface dipoles etc.). As a consequence and as found in our experiments the values of E_{PEII} are different for different technologies, samples, cleaning procedures even for so-called "same" passivation material. Furthermore as electron irradiation changes the surface conditions (as known from AES) the crossover energy is changed by irradiation (normally E_{PEII} decreases a little bit).

J. Reimer: What means of reducing the primary beam current did you use? Was it accomplished by reducing the beam diameter or could it be controlled independent of that?

Authors: As discussed for different e-beam test techniques in the paper, reducing the primary electron current density is possible by increasing the scanned area, reducing the beam current, chopping the beam at low duty cycles (1/100 - 1/1000) or defocussing the spot of the beam. Which way is chosen depends on the applied test techniques and the necessary time- and voltage resolution and spot size.

J. Reimer: Can you provide results or estimates of the percent error in capacitive coupling voltage measurements for different ratios of spacing/passivation thickness, i.e. 0.9:1.0; 1.0:1.0; 1.5:1.0; 2.0:1.0; 2.5:1.0?

Authors: The measurement error occuring when using the capacitive coupling voltage contrast depends on three factors: 1) incomplete coupling of the applied voltage to the passivation surface depending on device geometrie including passivation thickness 2) influence of the microfield on secondary electron trajectories 3) loss of signal due to electron irradiation.
Point 3 is discussed in this paper. Numerical simulations concerning point 1, were done also showing how the coupled voltage is influenced by the ratio of electrode spacing and passivation thickness. A part of these results will be published at the Microcircuit Engineering Conference this year by Mr. Herrmann. At present we are working at the measurement error due to the microfield effect (point 3).

J. Reimer: What is the linearity of measured voltage values using CCVC?

Authors: As demonstrated by Fig. 19, the linearity of a waveform measurement is better than 10%, but it strongly depends on the ratio T_p/T_{dark} as discussed in Fig. 9 and in Eq. 8.